EDGE ARTICLE

Check for updates

Direct heteroarylation polymerization: guidelines for defect-free conjugated polymers†

Thomas Bura,‡[a] Serge Beaupré,‡[a] Marc-André Légaré,[b] Jesse Quinn,[c]
Etienne Rochette,[b] J. Terence Blaskovits,[a] Frédéric-Georges Fontaine, [iD][b]
Agnieszka Pron,[d] Yuning Li[c] and Mario Leclerc [iD] *[a]

Direct (hetero)arylation polymerization (DHAP) has emerged as a valuable and atom-economical alternative to traditional cross-coupling methods for the synthesis of low-cost and efficient conjugated polymers for organic electronics. However, when applied to the synthesis of certain (hetero)arene-based materials, a lack of C–H bond selectivity has been observed. To prevent such undesirable side-reactions, we report the design and synthesis of new, bulky, phosphine-based ligands that significantly enhance selectivity of the DHAP process for both halogenated and non-halogenated electron-rich and electron-deficient thiophene-based comonomers. To better understand the selectivity issues, density functional theory (DFT) calculations have been performed on various halogenated and non-halogenated electron-rich and electron-deficient thiophene-based comonomers. Calculations showed that the presence of bromine atoms decreases the energy of activation (E_a) of the adjacent C–H bonds, allowing undesirable β-defects for some brominated aromatic units. Both calculations and the new ligands should lead to the rational design of monomers and methods for the preparation of defect-free conjugated polymers from DHAP.

1. Introduction

Conjugated polymers are the object of considerable attention from both academic and industrial laboratories. They often combine the excellent electrical and optical properties of metals and inorganic semiconducting materials with the mechanical flexibility, simple processing, and low production cost of synthetic polymers. Their good solubility facilitates large-scale processing techniques such as roll-to-roll printing, which makes low-cost printed electronic device fabrication possible. Polymer solar cells (PSCs)[1–4] and organic field-effect transistors (OFETs)[5–9] are among the most promising applications for conjugated polymers. With power conversion efficiencies having surpassed 10%,[10–12] lifetimes of nearly 15 years[13,14] and hole mobilities up to 36 cm^2 V^{-1} s^{-1},[15] conjugated polymers

seem to have now reached the requirements for commercial applications.[16,17]

The development of plastic electronics relies on innovative, robust and versatile coupling methods, such as Ziegler–Natta,[18,19] Migita–Stille,[20] Kumada,[21] Heck,[22] Miyaura–Suzuki,[23] Negishi[24] and olefin-metathesis[25–27] to produce well-defined conjugated polymers. However, production cost, presence of impurities, batch-to-batch variations and industrial scalability are still major issues for the implementation of plastic electronics. For instance, Migita–Stille cross-coupling polymerization techniques, which involve the use of organostannanes (synthesized *via* multistep organometallic processes that require demanding purification steps), lead to stoichiometric quantities of toxic by-products such as Me$_3$SnBr. Clearly, cheaper and more atom-efficient methodologies are highly desirable for the preparation of semiconducting organic polymers and their large-scale applications.

For these reasons, direct (hetero)arylation polymerization (DHAP) is generating great interest among the polymer science community and is now considered an important asset for polymer chemists despite the early stage of its development.[28–34] Tracing its origins to the synthesis of small organic molecules by direct (hetero)arylation, this polymerization method facilitates C–C bond formation between (hetero)arenes and (hetero)aryl halides (most commonly I and Br) catalyzed by palladium complexes. Unlike the Migita–Stille cross-coupling polymerization, only benign by-products are generated during the DHAP (mainly CsHCO$_3$ and CsBr). Up to now, this polymerization

[a]*Canada Research Chair on Electroactive and Photoactive Polymers, Department of Chemistry, Université Laval, Quebec City, Quebec, G1V 0A6, Canada. E-mail: Mario.Leclerc@chm.ulaval.ca*

[b]*Department of Chemistry, Université Laval, Quebec City, Quebec, G1V 0A6, Canada*

[c]*Department of Chemical Engineering, University of Waterloo, Waterloo, Ontario, N2L 3G1, Canada*

[d]*Merck Chemicals Ltd, Chilworth Technical Centre, SO16 7QD, UK (A Subsidiary of Merck KGaA, Darmstadt, Germany)*

‡ T. Bura and S. Beaupré contributed equally.

method has been successfully applied to the synthesis of many conjugated polymers based on key monomers such as 3-alkylthiophene,[35–39] benzodithiophene (BDT),[40–42] 5-alkylthieno[3,4-c]pyrrole-4,6-dione (TPD)[43–46] and 3,6-bis(thiophen-2-yl)-2,5-bis(2-alkyl)pyrrolo[3,4-c]-pyrrole-1,4-dione (DPP)[47–54] derivatives.

Despite recent achievements, significant challenges, mainly for some thiophene-based derivatives that feature several active C–H bonds, remain to be overcome, namely: (1) α-α homocouplings side-reactions and (2) regioselectivity issues (α,β

Fig. 1 Most probable structural defects upon direct (hetero)arylation polymerization (DHAP).

activated hydrogen atoms) that lead to β-defects (see Fig. 1). Mechanistically speaking, direct (hetero)arylation involves the oxidative addition of an (hetero)arylhalide substrate to a palladium catalyst followed by the heterolytic cleavage of a C–H bond of a second (hetero)aryl substrate, leading to the formation a new C–C bond via reductive elimination. Most (hetero)arenes undergo a concerted metalation-deprotonation (CMD) process in which the co-ligand directly participates in the proton transfer.[30] Presently, a limited number of phosphine-based ligands yield high reactivity and selectivity for DHAP. Among them, $P(o\text{-NMe}_2(C_6H_4))_3$ has proven itself to be suitable to the preparation of highly regioregular poly(alkylthiophene)s while $P(o\text{-OMe}(C_6H_4))_3$ seems adequate for the copolymerization of bromoarenes with heteroarenes.[55] Inspired by the pioneering work done by Buchwald et al.[56] on the design of specific phosphine ligands (SPhos, XPhos, DavePhos, etc.) for palladium-catalyzed formation of C–C, C–N and C–O bonds and the studies by Thompson et al.,[57] Bura et al.[32] and Dubnik et al.[58] demonstrating the positive influence of bulky carboxylic acid additives on the DHAP selectivity, we report new phosphine-based ligands closely related to $P(o\text{-OMe}(C_6H_4))_3$ (L$_{REF}$, Fig. 2). The phosphines were made bulkier at the ortho-position (L1–L5) using a low cost, simple and efficient methodology in the hope that they will enhance DHAP selectivity. The effect of the phosphine-based ligands was investigated for the polymerization of various brominated and non-brominated electron-rich

Fig. 2 The chemical structures of the phosphines and comonomers studied in this work.

and electron-poor thiophene-based monomers (Fig. 2). The influence of the nature of the substituents was also analyzed. Finally, density functional theory (DFT) calculations were used to rationalize the selectivity issues observed for some halogenated and non-halogenated electron-rich and electron-deficient benzo[1,2-b:4,5-b′]dithiophene (BDT), pyrrolo[3,4-c]-pyrrole-1,4-dione (DPP) and thiadiazolo[3,4-e]isoindole-5,7-dione (TID) derivatives. DFT calculations were also utilized to explain why some well-defined and nearly defect-free conjugated polymers reported in literature were successfully prepared by DHAP.

2. Results and discussion

As reported in the ESI,† the reference copolymers were first synthesized using the well-established Migita–Stille cross-coupling polymerization using the following synthetic procedure: Pd_2dba_3/ligand (ratio 1 : 4) and equimolar amounts of comonomers in toluene at 110 °C led to polymers **P1S** to **P4S**. As shown in Table S2,† high number-average molecular weight

$(\overline{M}_n)$ of 56 and 57 kg mol^{-1} was obtained for **P1S** and **P3S** when triphenyl arsine (AsPh$_3$) was used as ligand for the Stille cross-coupling polymerization.[59] Unlike **P1S** and **P3S**, the same catalytic system led to **P2S** and **P4S** with lower molecular weights. The molecular weight of **P2S** is limited due to its poor solubility (linear side chain on BDT). Indeed, regardless of the polymerization conditions, precipitation of the growing polymer chain occurs within few minutes. On the other hand, high molecular weight **P4S** (alkoxy side chain on BDT) can be obtained when P(o-Tolyl)$_3$ is used as ligand instead of AsPh$_3$. Indeed, $\overline{M}_n$ up to 150 kg mol^{-1} was reached, evidencing both the better efficiency of Pd_2dba_3/P(o-Tolyl)$_3$ catalytic system and the effect of the side chain on the of the BDT unit (alkoxy vs. alkyl). However the lack of solubility of the higher molecular weight batches led to broad and featureless ^{1}H NMR spectra. For comparison purposes in terms of molecular weights, Pd_2dba_3/AsPh$_3$ catalytic system was therefore used as reference. All polymers (soluble fraction after Soxhlet extractions) obtained by Migita–Stille cross-coupling polymerization are soluble in chlorinated solvents such as
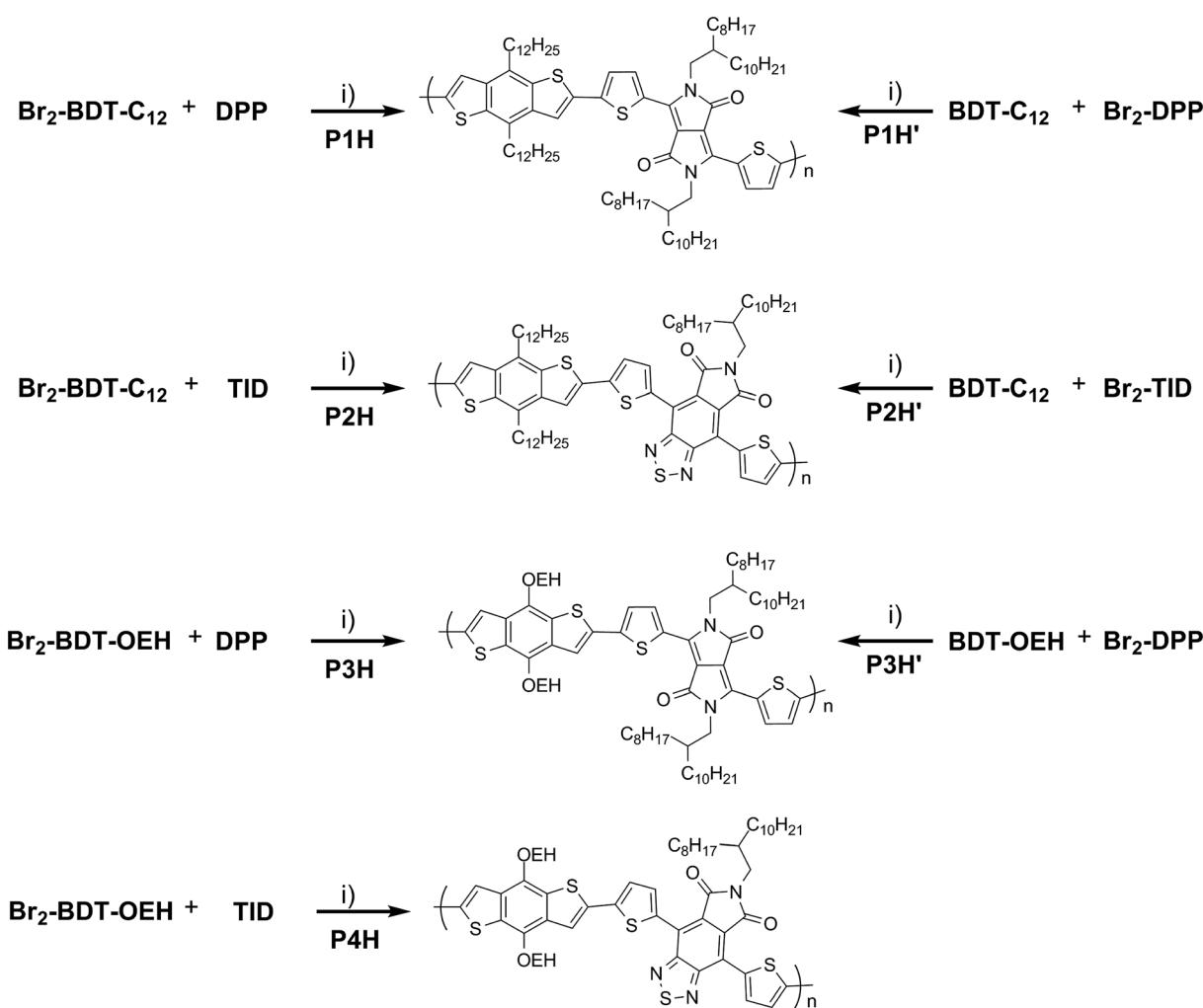
Condition: i) Pd(OAc)$_2$ (5 % mol), ligand (20 % mol), Cs$_2$CO$_3$ (3eq.), pivalic acid (PivOH, 1eq.), toluene 125°C

Scheme 1 Synthetic routes for **P1H** to **P4H** and **P1H′** to **P3H′** by DHAP.

chloroform, o-dichlorobenzene, 1,2,4-trichlorobenzene and 1,1,2,2-tetrachloroethane. In order to implement new DHAP protocols, the new phosphine-based ligands were easily prepared from a modified two-step synthetic procedure derived from Takeda *et al.*[60] using commercially available 2-bromophenol. Simple recrystallization of the crude reaction mixture using an ethyl ether/methanol solution led to the isolation of pure crystalline phosphines with overall yields of 40–60% (see ESI†). The chemical structures of these new phosphines have been determined by ^{1}H, ^{13}C and ^{31}P nuclear magnetic resonance spectroscopies and X-ray crystallography (for **L4** and **L5**) (see ESI†).

We first evaluated the polymerization of Br$_2$-BDT-C$_{12}$ (a halogenated electron-rich thiophene-based derivative with chemically reactive β-C–H bonds) with DPP (a non-halogenated electron-poor thiophene-based derivative with reactive α and β C–H bonds), two highly-studied and efficient building blocks in organic electronics (Scheme 1). γ-C–H bonds on DPP are inactive to C–H activation due to steric hindrance.[47,61] The copolymerization of these units yielded **P1H**. On the basis of previous studies[32,62] and as a reference point for comparison purposes, we kept the following polymerization conditions constant throughout this study: to a 0.5 mol L^{-1} solution of the monomers in toluene were added 5 mol% of Pd(OAc)$_2$, 20 mol% of phosphine, 3 equivalents of Cs$_2$CO$_3$, and 1 equivalent of pivalic acid (PivOH). The mixture was reacted at 125 °C (see Experimental details in ESI†). Polymerization using tris(o-methoxyphenyl)phosphine (**L$_{REF}$** in Fig. 2) was used as a control because of its generally satisfactory catalytic activity and selectivity in the DHAP (see ESI† for initial screening of DHAP conditions, Table S1†). The polymerization data are reported in Table S3† and the UV-Vis absorption spectra (in solution) of the resulting materials are shown in Fig. 3. For each ligand (**L1–L5**),

the polymerization proceeds as rapidly as when **P1H-L$_{REF}$** was utilized, and in order to limit unwanted side-reactions, each polymerization was stopped after one hour due to gelation of the reaction mixture.[62] The yields of polymerization (obtained for the soluble fraction collected after Soxhlet extraction) are around 75% for each entry. As reported in Table S3,† **P1H-L$_{REF}$** has lower number-average molecular weight ($\overline{M}_n$ = 21 kg mol^{-1}) than **P1S** ($\overline{M}_n$ = 56 kg mol^{-1}, obtained by Migita–Stille cross-coupling). Despite optimization of the polymerization parameters, the molecular weights of **P1H-L$_{REF}$** were systematically lower than that of **P1S**. In addition to large discrepancies between $\overline{M}_n$, the shape of the UV-Vis absorption spectrum of **P1H-L$_{REF}$** (λ_{max} = 753 nm) also differs from that of **P1S** (λ_{max} = 754 nm) (Fig. 3). More importantly, the absorption spectra for the **P1H** series show no sign of a shoulder near 820 nm. This shoulder was already observed by Janssen *et al.* for certain DPP-based polymers and was attributed to α-α homocoupling of DPP units.[63] One may take this absence of a shoulder in the UV-Vis spectra for **P1H-L1** to **L5** as indirect proof that this catalytic system reduces or inhibits the formation of such defects.[64] The UV-Vis absorption spectra also show that the vibronic bands centered at 690 nm and the broad shoulder near 630 nm do not have the same intensity for **P1H-L$_{REF}$** as for **P1S**. These spectroscopic observations suggest that while DHAP using tris(o-methoxyphenyl)phosphine (P(o-OMe$_3$(C$_6$H$_4$)$_3$)) may prevent homocoupling between DPP units, other side reactions such as BDT–BDT homocoupling or β-defects may still occur. However, those defects are difficult to assess even with the most advanced spectroscopic techniques and unfortunately, the NMR analyses performed for **P1H** series are ineffective for determining and characterizing the defects (β-defects or α-α homocouplings) embedded in the polymer due to broad and featureless signals. From Fig. 3, one can see that the replacement of the methyl group (**L$_{REF}$**) on the phosphine ligand by an isopropyl group (**L1**) has no positive effect on the catalytic activity (Table S3†): while the UV-Vis absorption spectra of **P1H-L1** is similar to **P1H-L$_{REF}$**, the molecular weight of **P1H-L1** is lower than that of both **P1H-L$_{REF}$** and **P1S**. However, increasing the steric bulkiness of the phosphines (**L2–L5**) led to a significant improvement of both the molecular weight and regioregularity of the BDT–DPP copolymers (Fig. 3 and Table S3†). $\overline{M}_n$ over 39 kg mol^{-1} were obtained for **P1H-L2** to **L5** series which are nearly twice the values obtained for **P1H-L$_{REF}$** and **P1H-L1**. UV-visible absorption spectra of **P1H-L2** to **P1H-L5** also differ from **P1S**, **P1H-L$_{REF}$** and **P1H-L1** suggesting that the bulky phosphines can influence the resulting chemical structure of the polymers obtained (Fig. 3a and b). A bathochromic shift (up to 4 nm) of the absorption maxima was observed for **P1H-L2** to **P1H-L5** when compared to **P1S**, **P1H-L$_{REF}$** and **P1H-L1**. Since $\overline{M}_n$ values of **P1H-L2** to **P1H-L5** are lower than that of **P1S**, one may conclude that the slight bathochromic shift observed may originate from an increased regioregularity along the conjugated backbone. These results clearly show that when the bulkier phosphines are used, the vibronic band (690 nm) has the same intensity as that observed for **P1S**, while the shoulder centered at 820 nm (ascribed to DPP–DPP homocoupling) is absent. Despite the lack of clear and well defined NMR spectra, these first experiments indicate
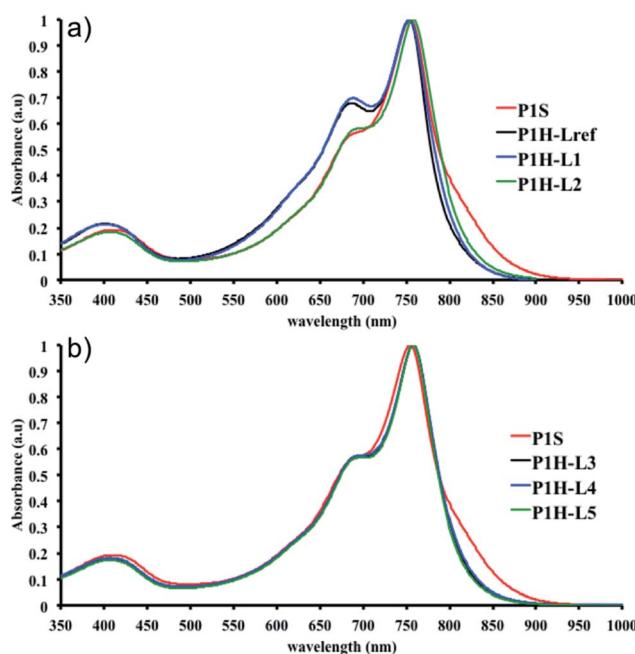
Fig. 3 UV-Vis spectra of **P1S** and **P1H** series (solution in CHCl$_3$).

that increasing the steric hindrance of the phosphine alkoxy chains can improve the selectivity over the widely used $P(o\text{-}OMe(C_6H_4))_3$ for the copolymerization of a halogenated electron-rich thiophene-based derivative (Br_2-BDT-C_{12}) with a non-halogenated electron-poor thiophene-based moiety (DPP).

In the absence of well-defined NMR data, organic field-effect transistors (OFETs) (see ESI†) were utilized to probe electrical properties of polymers. Indeed, while the performance of such devices depend on tedious processing optimization steps and while OFETs measurements will not allow the accurate identification or quantification of the defects (β-defects or α-α homo-couplings), the charge mobility in the devices is still expected to be affected by defects in the polymer (Table 1). In this study, **P1S** was used as a benchmark (even though the presence of DPP–DPP homocoupling within the main chain is suspected) and was compared to **P1H-L$_{REF}$**, **P1H-L3** and **P1H-L4**. All polymers showed ambipolar behavior. As reported in Table 1, the OFET results are in good agreement with the UV-Vis absorption data for the **P1H** polymer series. Based on the above, **P1H-L$_{REF}$** (low molecular weight and different UV-Vis absorption spectra as compared to **P1S**) is the least efficient material. On the other hand, both **P1H-L3** and **P1H-L4** (higher molecular weights and displaying a good overlap of the UV-Vis absorption spectra without the shoulder at 820 nm) led to average hole and electron mobilities at least as good as than those measured for **P1S** and better than those of **P1H-L$_{REF}$**. It is worth noting that the average hole mobilities obtained for the **P1H** series are in the same range as those reported by Morse *et al.*[65] All these results suggest that bulky phosphine ligands result in well-defined

BDT–DPP copolymers with fewer defects than those obtained by Migita–Stille polymerization.

To validate this hypothesis, we then applied this catalytic system to the synthesis of a copolymer containing a promising electron-deficient moiety studied in organic electronics: bis(thiophen-2-yl)-6-(2-octyldodecyl)-[1,2,5]thiadiazolo[3,4-*e*]isoindole-5,7-dione (TID) (Fig. 2).[66–68] The experimental conditions in this study were the same as those used for the **P1H** series. The polymerization data are summarized in Table S4† and the UV-Vis absorption spectra are shown in Fig. 4. The effect of the bulkiness of the phosphine for **P2H** was the same as **P1H**. Both polymerization times and yields (around 75%) are similar for most of the ligands except for **P2H-L$_{REF}$** where the yield of the soluble fraction was reduced to 39%. As observed for the **P1H** series, the bulkiest phosphine (**L4**) led to the highest number-average molecular weight (**P2H-L4**, 21 kg mol^{-1}). Fig. 4 shows that the UV-Vis absorption spectra of both **P2H-L$_{REF}$** and **P2H-L1** are quite different from that of **P2S**. While the band gaps (E_g = 1.48 eV) are similar, the vibronic bands of the polymer prepared by the different polymerization methods do not overlap one another. Although **P2H-L$_{REF}$** and **P2H-L1** have the same number-average molecular weight ($\overline{M_n}$ = 14 kg mol^{-1}), the overall shape of the UV-Vis absorption spectra are also different. A substantial shift of the absorption maximum (up to 8 nm) was observed for **P2H-L1** relative to **P2H-L$_{REF}$**. This behaviour indicates improved regioregularity of **P2H-L1**. Furthermore, **L3**, **L4** and **L5** led to better molecular weights and regioregularity of the BDT–TID copolymer (Table S4;† Fig. 4). **P2H-L3**, **P2H-L4** and **P2H-L5** show a small bathochromic shift of the maximum of absorption (up to 2 nm) when compared to **P2S**. As with the **P1H** series, since the molecular weight of each entry is comparable, one can assume that the slight

Table 1 Charge carrier mobilities of polymers in BGBC OFETs

	P type	N type
	Average (±standard deviation) hole mobility^a, cm^2 V^{-1} s^{-1}	Average (±standard deviation) electron mobility^a, cm^2 V^{-1} s^{-1}
P1S	3.8 (±0.8) × 10^{-2}	4.0 (±0.2) × 10^{-3}
P1H-L$_{REF}$	4.3 (±0.1) × 10^{-3}	1.9 (±0.1) × 10^{-3}
P1H-L3	1.5 (±0.9) × 10^{-3}	1.0 (±0.4) × 10^{-3}
P1H-L4	9.0 (±0.2) × 10^{-3}	8.3 (±0.1) × 10^{-3}
P2S	3.1 (±0.7) × 10^{-2}	2.0 (±0.1) × 10^{-3}
P2H-L$_{REF}$	1.2 (±0.1) × 10^{-2}	1.5 (±0.2) × 10^{-3}
P2H-L3	1.3 (±0.3) × 10^{-2}	3.7 (±0.3) × 10^{-4}
P2H-L4	2.5 (±0.2) × 10^{-2}	1.4 (±0.1) × 10^{-3}
P2H-L5	2.0 (±0.3) × 10^{-2}	2.4 (±0.5) × 10^{-3}
P3S (High $\overline{M_n}$)	1.4 (±0.2) × 10^{-3}	2.9 (±0.5) × 10^{-4}
P3S (Low $\overline{M_n}$)	8.0 (±0.9) × 10^{-4}	9.4 (±0.3) × 10^{-5}
P3H-L$_{REF}$	1.2 (±0.1) × 10^{-4}	1.2 (±0.1) × 10^{-3}
P3H-L4	2.0 (±0.4) × 10^{-4}	4.3 (±0.1) × 10^{-5}
P3H-L5	6.2 (±0.1) × 10^{-5}	8.0 (±0.1) × 10^{-5}
P4S-High	2.5 (±0.9) × 10^{-4}	4.5 (±1.1) × 10^{-4}
P4H-L2	8.7 (±1.0) × 10^{-5}	2.3 (±1.1) × 10^{-4}
P4H-L4	7.5 (±2.5) × 10^{-5}	1.6 (±0.6) × 10^{-4}
P4H-L5	5.4 (±0.7) × 10^{-5}	5.6 (±2.8) × 10^{-4}

^{a} The average (±standard deviation) mobilities were obtained in the saturation regime from at least five devices for each condition.
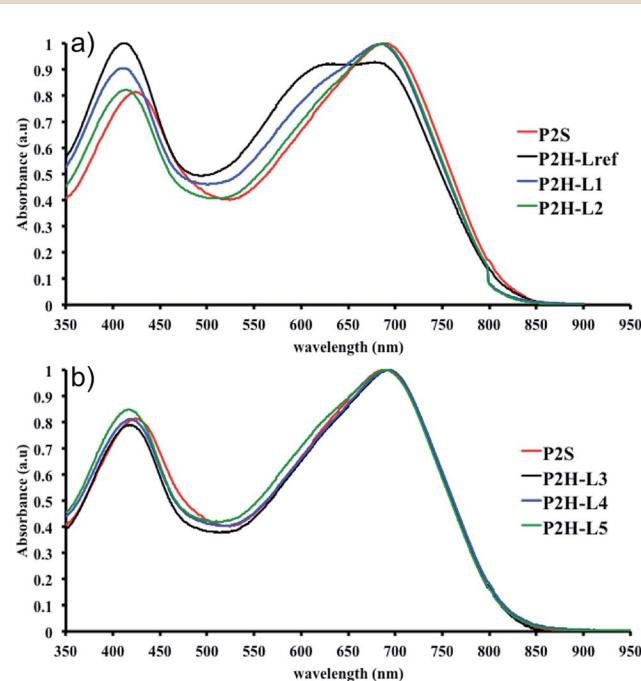
Fig. 4 UV-Vis spectra of **P2S** and **P2H** series (solution in CHCl$_3$).

bathochromic shift observed for **P2H-L3** to **L5** to be the result of a more regioregular structure.

Fortunately, well-defined ^{1}H NMR spectra were obtained for this series. The ^{1}H NMR spectra of each monomer and polymer were obtained in deuterated 1,1,2,2-tetrachloroethane ($C_2D_2Cl_4$) at 90 °C using the same acquisition parameters. In order to assign the signals and to identify defects (*i.e.* α-α homocouplings) homopolymers of BDT and TID were prepared as model compounds (see ESI†). Fig. 5 highlights the aromatic region of the ^{1}H NMR spectra of **P2S**, **P2H-L$_{REF}$**, **P2H-L2** and **P2H-L4**. For each polymer, the main peaks A, B and C correspond to the protons of the main chain while the residual signals (a–h) are attributed to end groups or α-α homocoupling units (see ESI†). These spectra show for **P2H-L2** and **P2H-L4**, a significant drop of the intensity of the peak at 8.21 ppm (a) (related TID–TID homocoupling) and of the shoulder near 7.7 ppm (c) (related to BDT–BDT homocoupling). For these two polymers, similar UV-Vis absorption spectra were obtained, indicating that the bulkier phosphines limit side reactions, particularly α-α

homocouplings. As with the **P1H** series, OFET measurements were used to evaluate the performance of the **P2H** series, with **P2S** being used as a benchmark (Table 1). With the exception of the lower electron mobility observed of **P2H-L3**, the overall performance of the **P2H** series is comparable to that of the reference polymer **P2S**. The overall OFET performance of the **P2H** series combined with the UV-Vis and ^{1}H NMR spectra tend to show once again that the bulkier phosphine leads to better materials with fewer defects when compared to **P2S**.

To push further our investigation, we then applied our catalytic system to the polymerization of Br$_2$-BDT-OEH and DPP. As mentioned in the Introduction, the main objective was to evaluate if the electronic structure of the BDT side chain affects the reactivity and selectivity of the DHAP. The polymerization data are summarized in Table S5† and UV-Vis absorption spectra are shown in Fig. 6. Unlike **P1H** and **P2H** series, both $\overline{M}_n$ and polymerization yields (about 30%, soluble fraction recovered after Soxhlet extractions) of **P3H** series were lower than those obtained for **P3S** (Table S5†). For each entry, the
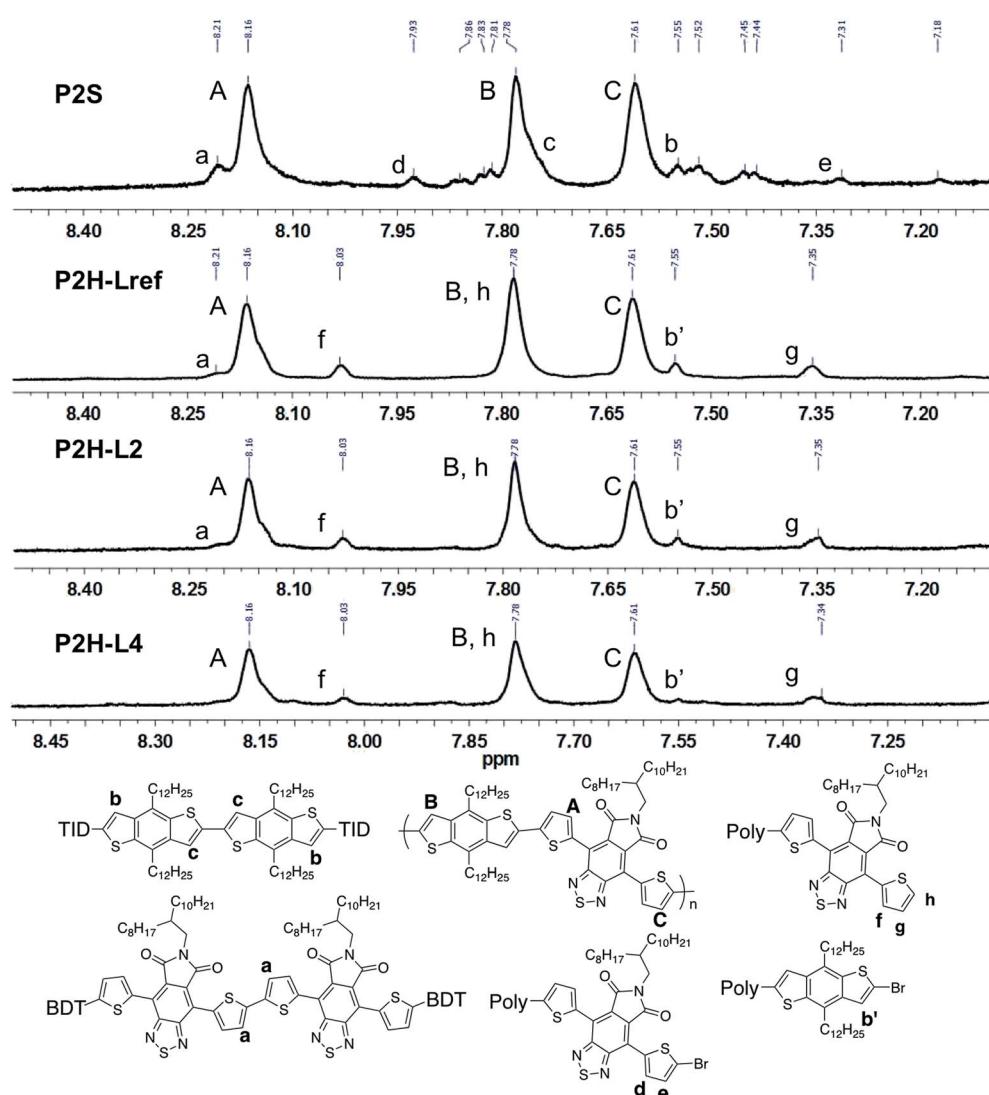

**Fig. 5** ^{1}H NMR spectra of **P2S**, **P2H-L$_{REF}$**, **P2H-L2** and **P2H-L4**.
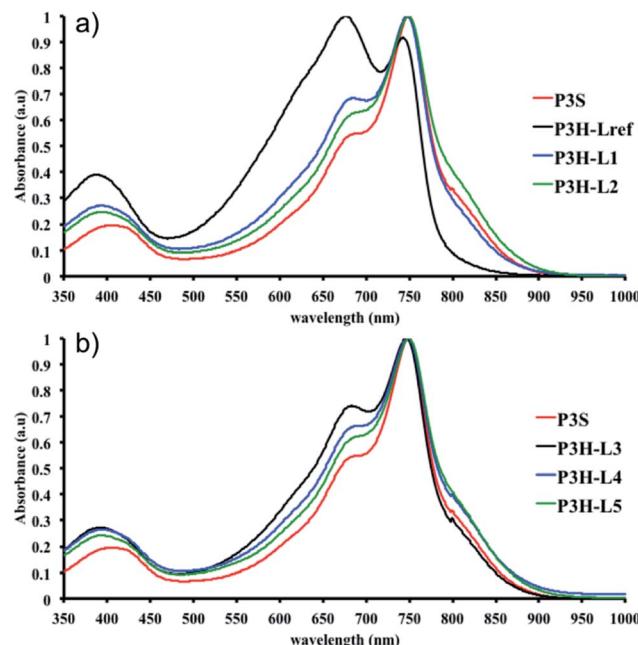
Fig. 6 UV-Vis spectra of **P3S** and **P3H** series (solution in CHCl$_3$).

polymerization was terminated after 2 hours due to gelation of the reaction mixture. Longer polymerization times did not lead to higher molecular weights. Moreover, as shown in Fig. 6, UV-Vis absorption spectra clearly demonstrate that the **P3H** series, regardless of the ligand, are not the same materials as **P3S** and the discrepancy between the UV-Vis spectra cannot be explained by the lower molecular weights alone. While no DPP–DPP homocoupling can be observed for **P3H-L$_{REF}$** (indicated by the absence of a shoulder at 820 nm), the shift of the absorption maximum (centered at 660 nm) indicates that the chemical structure of the conjugated skeleton differs from that of **P3S** and may be a result of lower DHAP selectivity between Br$_2$-BDT-OEH and DPP. Upon increasing the bulkiness of the alkoxy chain on the phosphine, the overall shape of the UV-Vis spectra approached that of **P3S** (Fig. 6). A maximum of absorption was found at 677 nm with a vibronic band at 740 nm for **P3H-L$_{REF}$**, while absorption maxima at 748 and 750 nm were observed for **P3HL1-L2** and **P3HL3-L5**, respectively, with a vibronic band at 685 nm. Based on these results, it seems that the alkoxy side chains on BDT modify the electronic properties of the monomer and affect the reactivity compared to **P1H** series. ^{1}H NMR spectra were fruitless in determining the nature of the defects present in the **P3S** and **P3H** series due to broad and featureless signals. As with **P1H** and **P2H**, OFET measurements were performed. **P3S** was used as a benchmark and compared to **P3H-L$_{REF}$**, **P3H-L4** and **P3H-L5** (Table 1). With the exception of the electron mobility of **P3H-L$_{REF}$** (the least well-defined polymer as determined from absorption spectra), the overall performance of the **P3H** series were one to two orders of magnitude lower than the reference polymer.

In order to verify that the electronic nature of the side chain installed on BDT moiety does affect the selectivity of the DHAP, we applied this catalytic system to the polymerization of Br$_2$-

BDT-OEH and TID (**P4H** series, Scheme 1). The polymerization data are summarized in Table S6† and UV-Vis absorption spectra are shown in Fig. 7. Molecular weights (from soluble fraction recovered after Soxhlet extraction) of the polymers obtained by the DHAP were lower than those obtained for **P4S**-High ($\overline{M}_n$ of 30 kg mol^{-1}) except for **P4H-L2** ($\overline{M}_n = 27$ kg mol^{-1}) and **P4H-L4** ($\overline{M}_n = 30$ kg mol^{-1}). Unlike **P4S**, the kinetics of DHAP was slow and no improvement of molecular weights was observed for longer polymerization times. Moreover, to eliminate the effect of molecular weight discrepancies during polymer comparison experiments, we also prepared **P4S**-Low, a low molecular weight batch ($\overline{M}_n = 16$ kg mol^{-1}) similar to those obtained for **P4H-L1**, **L3** and **L5**. As shown in Fig. 7, the mismatch of all the UV-Vis absorption spectra of **P4H** series compared to **P4S**, combined with the shift of the intensity of the two main bands (400 nm and 640 nm) raises concerns as to the nature of the BDT side chain on the DHAP selectivity. **P4S**-High exhibits two maxima of absorption, one centered at 418 nm and another of higher intensity at 639 nm. These two maxima were observed at 414 nm and 617 nm for **P4S**-Low, indicating clear relationship between molecular weights and optical properties for **P4S**. As shown in Fig. 7a, the least comparable polymer was **P4H-L$_{ref}$**, with a number-average molecular weight of 10 kg mol^{-1} and an UV-Vis absorption spectrum with two blue-shifted maxima (407 and 583 nm) compared to **P4S**-Low (414 and 617 nm). Another striking feature, aside from the hypsochromic shift, is the inversion of the intensity of the two maxima observed for **P4H-L$_{ref}$**. This clearly indicates that the chemical structure of the conjugated backbone of **P4H-L$_{ref}$** is not the same as **P4S** (High and Low). Moreover, despite similar number-average molecular weight when compared to **P4S**-High ($\overline{M}_n = 30$ kg mol^{-1}), **P4H-L2** ($\overline{M}_n = 27$ kg mol^{-1}) and **P4H-L4** ($\overline{M}_n = 30$ kg mol^{-1}) also show hypsochromic shifts for both absorption
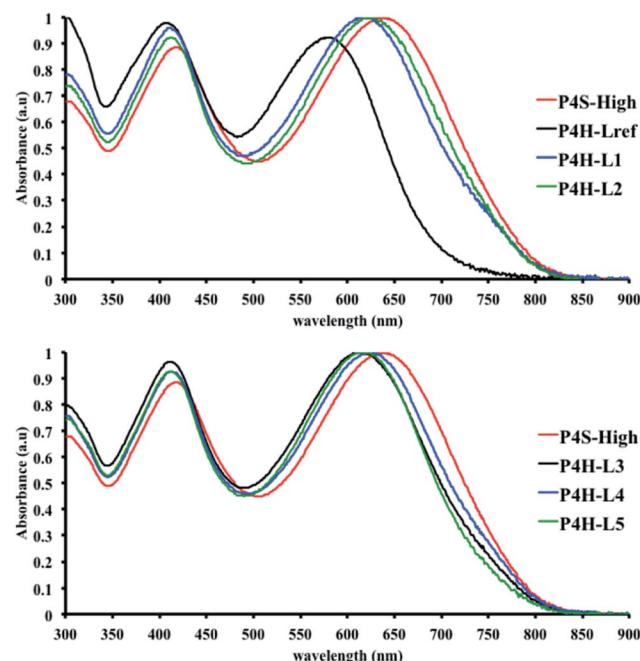

Fig. 7 UV-Vis spectra of **P4S** and **P4H** series (solution in CHCl$_3$).

bands, which also indicates the presence of defects within the main chain, as observed for the **P3H** series. Consistently with the fact that mismatches of the UV-Vis spectra between **P4S** and **P4H** series have been observed, lower OFETs performance for **P4H** series have been measured by experimental data (one order of magnitude lower than the reference polymer, see Table 1).

Well-defined ¹H NMR data were also obtained for **P4H**. Fig. 8 highlights the aromatic region of the ¹H NMR spectra of **P4S**, **P4H-L_REF**, **P4H-L2** and **P4H-L4**. On the basis of model compounds (see ESI†), the main peaks A, B and C correspond to the protons of the main chain while the residual signals (a–k) are related to end groups or homocoupling units. Although the exact integrations were difficult to determine, the lower intensity of the signal at 8.21 ppm for **P4H-L_REF** compared to the one observed for **P4S** suggests that the DHAP may lead to lower amounts of TID–TID homocoupling side-reactions. Moreover, for **P4H-L2** and **P4H-L4**, a significant drop of the intensity of the peak at 8.21 ppm (a) (related to the homocoupling of TID) was observed compared to **P4S**. The other residual peaks (h: 7.77 ppm; f: 8.03 ppm; g: 7.35) for **P4H-L2** and **P4H-L4** are less intense compared to **P4H-L_REF** due to higher molecular weights.

To rationalize this experimental data, DFT calculations at the B3LYP/TZVP (DZVP for palladium) level have been carried out to evaluate the activation barrier of the C–H bond activation of the CMD pathway. This method has been previously successfully applied to the rationalization and prediction of the regioselectivity of direct (hetero)arylation reactions on different arenes and heteroarenes.[69] It is worth noting these calculations are
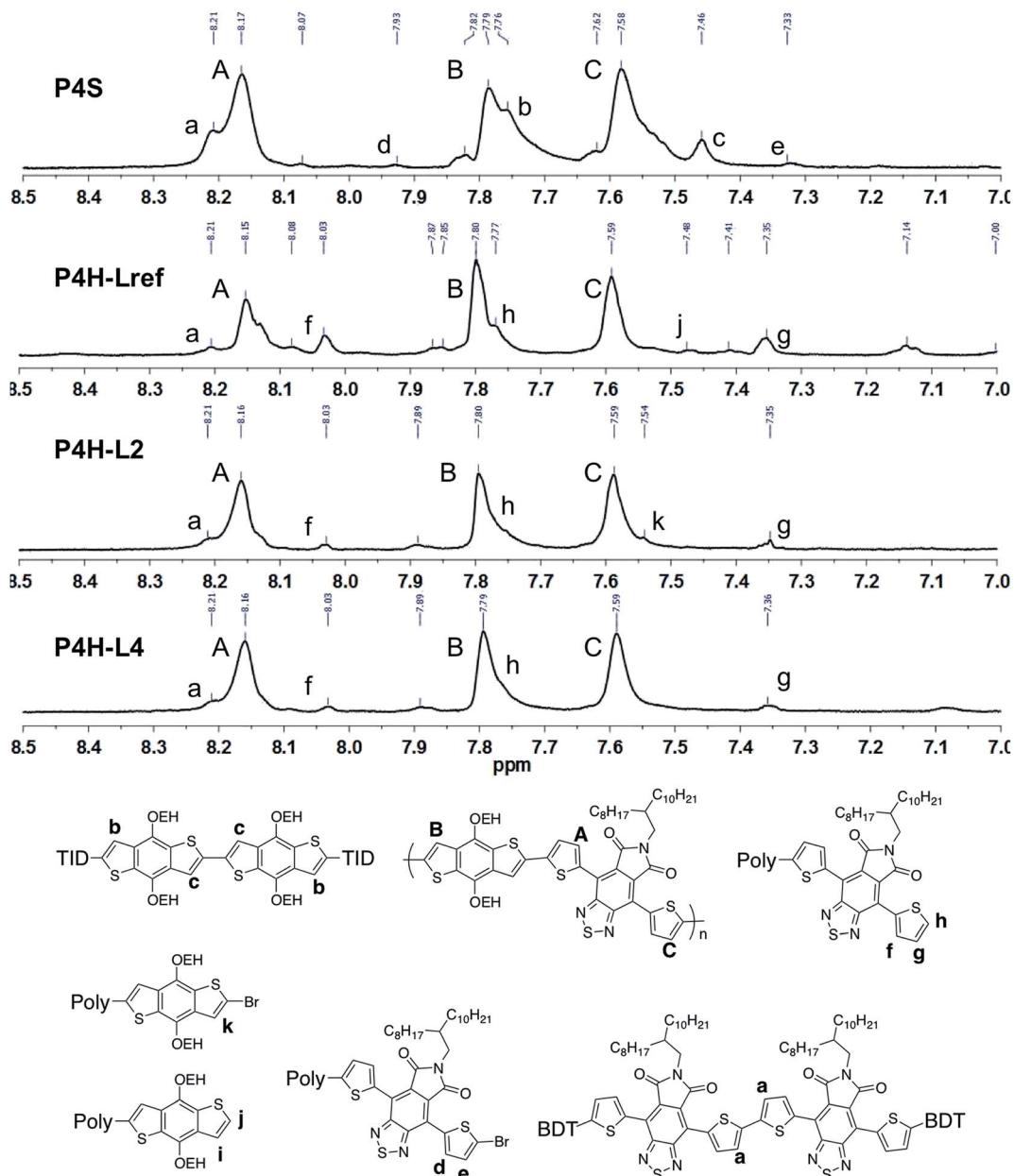
Fig. 8 ¹H NMR spectra of P4S, P4H-L_REF, P4H-L2 and P4H-L4.

relevant to α *versus* β selectivity for possible β-defects but does not say anything about potential α-α homocouplings. The model palladium catalyst $(PMe_3)Pd(Ph)(CH_3COO–)$ was used as a platform to calculate the Gibbs free energy of the CMD transition state associated to the activation of the different C–H bonds of each substrate (see Fig. 9 and ESI†). The results obtained using this approach are given in the following test using this notation: the activation energy (E_a) refers to the Gibbs free energy of the CMD transition state referenced to the substrate and model catalyst ($\Delta G_{298}^{\ddagger}$). Thus, in the case of DPP, the difference in the activation energy (ΔE_a) between H_α and H_β for the DPP moiety is found to be 4.4 kcal mol^{-1} (24.5 *vs.* 28.9 kcal mol^{-1}, respectively). Accordingly, it is possible to tentatively estimate (using Arrhenius's law) a selectivity ratio of the α-position at 125 °C (the temperature of polymerization). For this system, a ratio of about 250 : 1 favoring H_α can indeed be calculated for the DPP unit. On the other hand, the E_a of the H_β of the Br_2-BDT-C_{12} is 28.2 kcal mol^{-1} whereas the E_a for H_β on the Br_2-BDT-OEH is only 26.7 kcal mol^{-1}. It is worth noting that the theoretical calculations show that the electronic nature of the side-chains installed on BDT unit modifies the energy of activation of both α and β protons. Using these values, the ΔE_a between H_α of DPP (24.5 kcal mol^{-1}) and the H_β of the Br_2-BDT-OEH (26.7 kcal mol^{-1}) and Br_2-BDT-C_{12} (28.2 kcal mol^{-1}) are respectively of 2.2 and 3.7 kcal mol^{-1}, giving respective selectivity of about 15 : 1 and 100 : 1 at 125 °C. Although the 1.5 kcal mol^{-1} difference might look small, it indicates that the activation of the H_β of the Br_2-BDT-OEH will occur about one order of magnitude faster than the one of the H_β of the Br_2-BDT-C_{12} resulting in more β-defects, while the polymer using Br_2-BDT-C_{12} will better behave. This is in fair agreement with the UV-Vis absorption spectra observed for the **P1H** and **P3H** series, respectively.

For **P4H** (Br_2-BDT-OEH with TID), the difference in the energy of activation (ΔE_a) between H_α and H_β for the TID moiety is 4.7 kcal mol^{-1} (29.3–24.6 kcal mol^{-1}). For this system, a ratio of about 400 : 1 favoring H_α has been calculated. However, the ΔE_a between H_α of TID (24.6 kcal mol^{-1}) and the H_β of the Br_2-BDT-OEH (26.7 kcal mol^{-1}) is 2.1 kcal mol^{-1} while the ΔE_a between H_α of TID (24.6 kcal mol^{-1}) and the H_β of the Br_2-BDT-C_{12} (28.2 kcal mol^{-1}) is 3.6 kcal mol^{-1}. As discussed earlier, one can think that β-defects on BDT moiety can be the main defect found in the **P4H** series whereas a better selectivity is anticipated for the **P2H** series.

To continue our investigation, we carried out the polymerization of monomers with the bromide function on the electron-deficient units. 4,8-Bis(didodecyl)benzo[1,2-*b*:4,5-*b'*]dithiophene (BDT-C_{12}) or 4,8-bis(2-ethylhexyloxy)benzo[1,2-*b*:4,5-*b'*]dithiophene (BDT-OEH) was therefore polymerized with 3,6-bis(5-bromo-thiophen-2-yl)-2,5-bis(2-octyldodecyl)pyrrolo[3,4-*c*]-pyrrole-1,4-dione (Br_2-DPP) or 4,8-bis(5-bromo-thiophen-2-yl)-6-(2-octyldodecyl)-[1,2,5]thiadiazolo[3,4-*e*]isoindole-5,7-dione (Br_2-TID) to obtain the **P1H'**, **P2H'** and **P3H'** series (Scheme 1). The polymerization data for **P1H'** are reported in Table S7† and the UV-Vis absorption spectra in solution are shown in Fig. 10. The polymerization times were longer and the yields (about 25–30%) of the soluble fraction of the polymers in chloroform were consistently lower relative to both the **P1H** series and **P1S**, regardless of the nature of the ligand. DHAP polymerizations were run for 12 hours for all examples. After Soxhlet extractions, a large quantity of insoluble material was recovered indicating possible side reactions. Despite several attempts, both $\overline{M_n}$ and
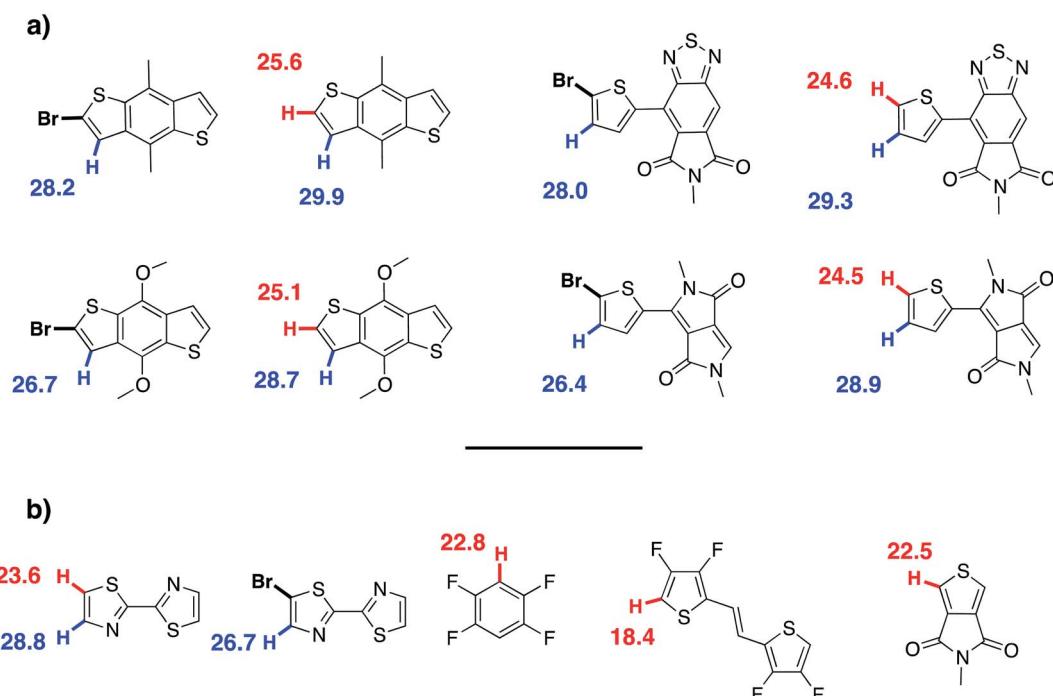

Fig. 9 The Gibbs free energy of the CMD transition state associated to the activation of α,β hydrogen atoms calculated by DFT.

Fig. 10 UV-Vis spectra of **P1S** and **P1H′** series (solution in CHCl₃).
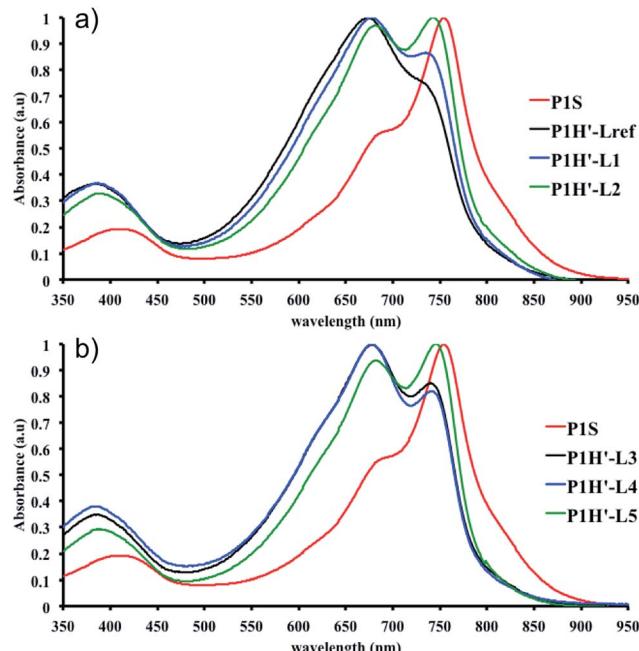

Fig. 11 UV-Vis spectra of **P2S** and **P2H′** series (solution in CHCl₃).

polymerization yield values were lower than those of the reference polymer **P1S**. As shown in Fig. 10, the UV-Vis absorption spectra of the **P1H′** series were different from the benchmark **P1S**. Clearly, this catalytic system did not yield the targeted polymers as opposed to the **P1H** series.

We then applied the catalytic system for the polymerization of 4,8-bis(didodecyl)benzo[1,2-*b*:4,5-*b*′]dithiophene (BDT-C₁₂) and 4,8-bis(5-bromo-thiophen-2-yl)-6-(2-octyldodecyl)-[1,2,5] thiadiazolo[3,4-*e*]isoindole-5,7-dione (Br₂-TID) **P2H′** (Scheme 1). The polymerization data for **P2H′** are reported in Table S8,† while the UV-Vis absorption spectra in solution are shown in Fig. 11. The polymerization times were generally longer and the yields (soluble fraction of the polymer in chloroform) lower compared to the **P2H** series and **P2S**. Like **P1H′** series, the UV-Vis absorption spectra obtained for **P2H′** were different from the reference, indicating, once again, that the targeted polymers were not obtained with this catalytic system.

As for the **P2H** series, well-defined ¹H NMR data were obtained for the **P2H′** samples in 1,1,2,2-tetrachloroethane (C₂D₂Cl₄) at 90 °C (see ESI, Section 4†). The shape of the UV-Vis absorption spectra of the **P2H′** series combined with ¹H NMR analyses confirm the presence of defects within the conjugated main chain. The same trend was observed for the copolymerization of BDT-OEH with Br₂-DPP (**P3H′** series, see Scheme 1). Lower molecular weights and yields were obtained with all phosphines (Table S9†). As with **P1H′**, a large quantity of insoluble material was recovered after Soxhlet extractions and the UV-Vis absorption spectra of the soluble fraction did not match that obtained for **P3S** (Fig. 12). In the light of the result obtained for the **P1H′**–**P3H′** series, we did not synthesize the **P4H′** series, *i.e.* the equivalent polymers to **P4H** with the bromide moiety on the electron-poor unit.
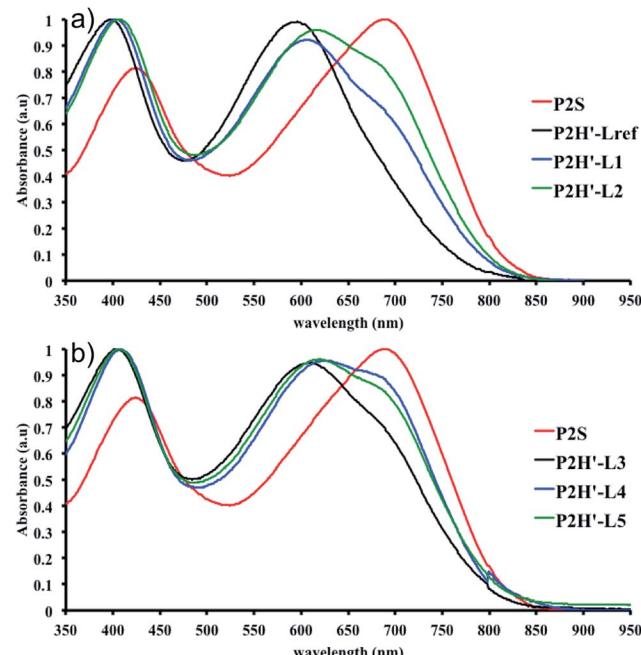
DFT calculations performed for **P1H′** (BDT-C₁₂ with Br₂-DPP) helped again to rationalize the experimental data obtained for this series (Fig. 9). Here, the ΔE_a between the H$_\alpha$ (25.6 kcal mol⁻¹) and H$_\beta$ (29.9 kcal mol⁻¹) of BDT-C₁₂ is 4.3 kcal mol⁻¹, indicating once again an excellent selectivity for the activation of H$_\alpha$. However, the ΔE_a between H$_\beta$ of the Br₂-DPP (26.4 kcal mol⁻¹) and H$_\alpha$ of the BDT-C₁₂ (25.6 kcal mol⁻¹) is only of 0.8 kcal mol⁻¹, suggesting poor selectivity and significant unwanted DPP–DPP β-defects.

For **P2H′** series (BDT-C₁₂ with Br₂-TID), the ΔE_a between H$_\alpha$ (25.6 kcal mol⁻¹) and H$_\beta$ (29.9 kcal mol⁻¹) of BDT-C₁₂ is 4.3 kcal mol⁻¹. On the other hand, the ΔE_a between H$_\beta$ of the Br₂-TID (28.0 kcal mol⁻¹) and H$_\alpha$ of the BDT-C₁₂ (25.6 kcal mol⁻¹) is 2.4 kcal mol⁻¹, leading to a 20 : 1 selectivity at 125 °C which would induce some TID–TID β-defects. The same trend was observed for the copolymerization between BDT-OEH with Br₂-DPP (**P3H′** series, see Scheme 1). Although the ΔE_a between H$_\alpha$ (25.1 kcal mol⁻¹) and H$_\beta$ (28.7 kcal mol⁻¹) of BDT-OEH of 3.6 kcal mol⁻¹ leads to a selectivity of about 100 : 1, the ΔE_a between H$_\beta$ of the Br₂-DPP (26.4 kcal mol⁻¹) and H$_\alpha$ of the BDT-OEH (25.1 kcal mol⁻¹) of 1.3 kcal mol⁻¹ gives a poor 5 : 1 selectivity, which would induce possible DPP–DPP β-defects. These observations are in good agreement with the experimental data obtained for **P3H′** series. Finally, according to the theoretical calculations, one can think that the synthesis of **P4H′** by DHAP (BDT-OEH with Br₂-TID) would also suffer from selectivity issues. Indeed, the ΔE_a between H$_\beta$ of the Br₂-TID (28.0 kcal mol⁻¹) and H$_\alpha$ of the BDT-OEH (25.1 kcal mol⁻¹) of 2.9 kcal mol⁻¹ gives a 40 : 1 selectivity, indicating possible TID–TID β-defects.

On the basis of these experimental-theoretical data, we extended the scope of our DFT calculations to other BDT and DPP-based copolymers recently synthesized by DHAP in order to
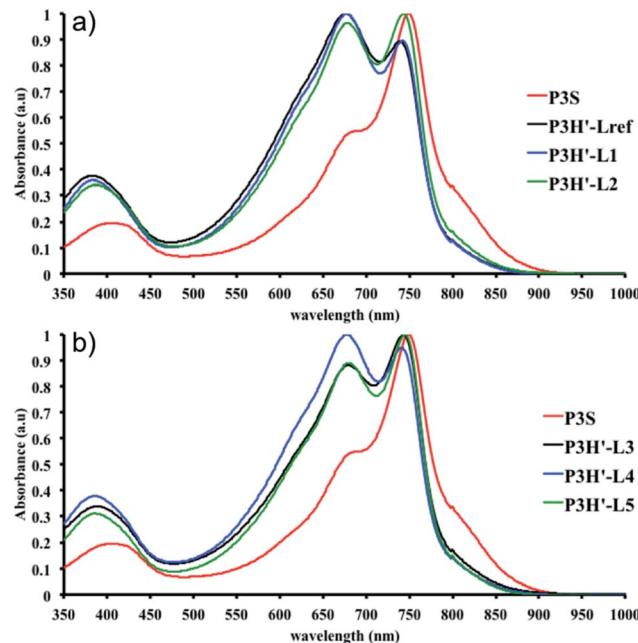
Fig. 12   UV-Vis spectra of P3S and P3H' series (solution in CHCl$_3$).

explain why some of them can be successfully prepared while other cannot. For instance, Li *et al.* reported that a relatively well-defined copolymer was obtained from the copolymerization of Br$_2$-DPP with bithiazole while poor performance was reported for the same copolymer synthesized using Br$_2$-bithiazole and DPP (Scheme 2a).[70] For the first case, the ΔE_a between the H$_\alpha$ (23.6 kcal mol^{-1}) and H$_\beta$ (28.8 kcal mol^{-1}) of bithiazole moiety is 5.2 kcal mol^{-1} which means that the activation of the H$_\alpha$ position is highly selective. Meanwhile, a selectivity of about 35 : 1 is observed when considering the ΔE_a value of 2.8 kcal mol^{-1} between H$_\beta$ of the Br$_2$-DPP (26.4 kcal mol^{-1}) and H$_\alpha$ of the bithiazole (23.6 kcal mol^{-1}). On the other hand, for the Br$_2$-bithiazole/DPP system, the ΔE_a between H$_\beta$ of the Br$_2$-bithiazole (26.7 kcal mol^{-1}) and the H$_\alpha$ of the DPP (24.5 kcal mol^{-1}) is only of 2.2 kcal mol^{-1} and should lead to less-defined structure. Wang and co-workers have also reported that the synthetic pathways used for the synthesis of DPP–tetrafluorobenzene (TFB) copolymer by DHAP affect the regioregularity of the resulting copolymer (see Scheme 2b) and, once again, the experimental data are in good agreement with the DFT calculations.[71] Indeed, for pathway A (DPP and Br$_2$-TFB), the ΔE_a between H$_\alpha$ and H$_\beta$ for the DPP moiety is 4.4 kcal mol^{-1} (24.5 *vs.* 28.9 kcal mol^{-1}, respectively) and leads to a selectivity ratio of
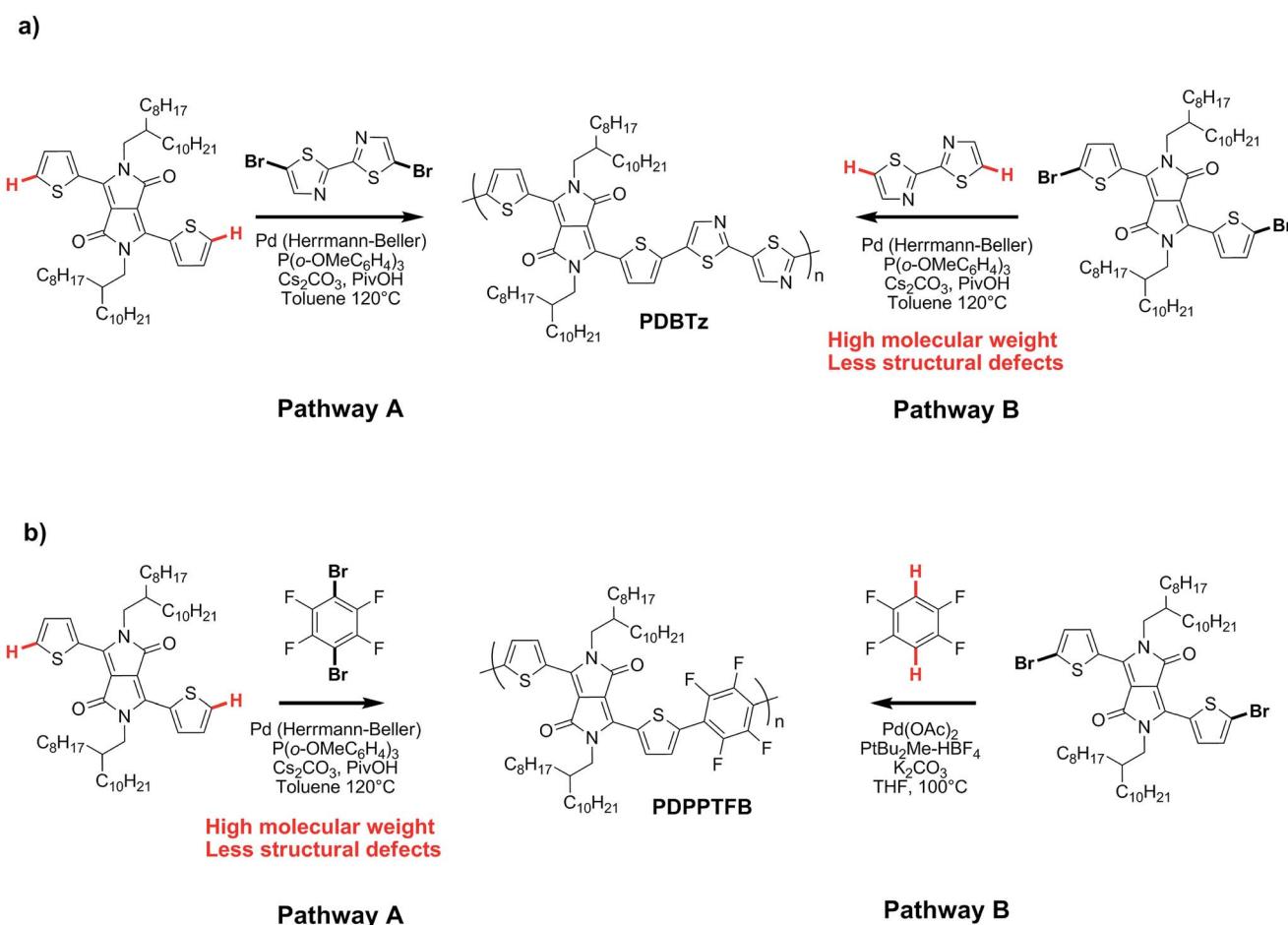
Scheme 2   Synthetic routes for (a) PDBTz and (b) PDPPTFB by DHAP.[70,71]

about 250 : 1. For the pathway B (see Scheme 2b), the ΔE_a between H_α of TFB (22.8 kcal mol^{-1}) and H_β on Br$_2$-DPP (26.4 kcal mol^{-1}) is 3.6 kcal mol^{-1}. According to these calculations, this means that some DPP–DPP β-defects might occur in the latter case. Along these lines, Wang *et al.* have reported the synthesis of PDPP-4FTVT for which experimental data once again are in good agreement with DFT calculations.[72] Indeed, 4FTVT comonomer has E_{a,H_α} of 18.4 kcal mol^{-1} (see Fig. 9) leading to a $\Delta H_\alpha - H_\beta$ of 8 kcal mol^{-1} with H_β of Br$_2$-DPP (26.4 kcal mol^{-1}). With an average hole and electron mobilities of 2.46 and 4.19 cm^2 V^{-1} s^{-1} respectively, those high values suggest that PDPP-4FTVT is a well-defined material. Finally, Marks *et al.*[58] and Farinola *et al.*[73] recently reported the synthesis of PBDTTPD by DHAP using Br$_2$-BDT-OEH and TPD as comonomers and obtained a polymer with similar properties than that one prepared from Stille coupling. DFT calculations can again explain these results. Indeed, for the TPD monomer with only one C–H bond available, an E_a of 22.5 kcal mol^{-1} was calculated (see Fig. 9). Thus, the ΔE_a between H_α of TPD (22.5 kcal mol^{-1}) and H_β on Br$_2$-BDT-OEH (26.7 kcal mol^{-1}) is 4.2 kcal mol^{-1} which should lead to a 200 : 1 selectivity ratio at 125 °C. All these calculations show that the choice of the comonomers is crucial for DHAP. Indeed, these calculations indicate that the presence of bromine atoms decreases the energy of activation (E_a) of the adjacent C–H bonds, allowing undesirable β-defects for some brominated aromatic units. However, some brominated monomers are not intrinsically inadequate but their utilization is strongly dependent upon the nature and reactivity of the respective comonomer. Finally, DFT calculations reported here show that most non-brominated thiophene-based building blocks have good selectivity at the α-positions.

3. Conclusion

In this study, we have shown that the selectivity of the direct heteroarylation polymerization (DHAP) of brominated electron-rich thiophene-based units and electron-deficient DPP and TID moieties can be significantly improved through a rational modification of the phosphine-based ligand. Indeed, five new phosphines with different *o*-substituent moieties (iso-propyl (**L1**), ethylhexyl (**L2**), cyclopentane (**L3**), cycloheptane (**L4**) and methylcyclohexane (**L5**)) have been synthesized and compared with tris(*o*-methoxyphenyl)phosphine. Selectivity enhancement was observed for bulkier phosphines, even preventing homo-coupling defects found in the Migita–Stille polymerization. Despite notable selectivity improvements, the utilization of hindered phosphines was not effective with some brominated thiophene-based comonomers. Theoretical calculations using DFT gave an estimation of the activation energies (E_a) for all possible C–H bonds to be activated during the CMD process and those calculations showed that the presence of a bromine atom decreases the energy of activation of the adjacent C–H bonds, potentially leading to undesirable competitive reactions. More importantly, the theoretical calculations tend to show that a careful choice of comonomers might be the key to obtain well-defined materials. This initial experimental-theoretical study is

part of a broader interest in mechanistic investigations in our laboratories. With this knowledge, we intend to develop a transition state to rationally design ligands and substrates for site-selective DHAP reactions. Finally, competition experiments on non-polymerizable model compounds could give some quantitative information and be compared to theoretical calculations.

References

1 A. Facchetti, *Chem. Mater.*, 2011, **23**, 733–758.
2 P.-L. T. Boudreault, A. Najari and M. Leclerc, *Chem. Mater.*, 2011, **23**, 456–469.
3 J. Chen and Y. Cao, *Acc. Chem. Res.*, 2009, **42**, 1709–1718.
4 I. Etxebarria, J. Ajuria and R. Pacios, *Org. Electron.*, 2015, **19**, 34–60.
5 Z. Bao, A. Dodabalapur and A. J. Lovinger, *Appl. Phys. Lett.*, 1996, **69**, 4108–4110.
6 A. Facchetti, *Mater. Today*, 2007, **10**, 28–37.
7 H. Sirringhaus, *Adv. Mater.*, 2014, **26**, 1319–1335.
8 Y. Xu, C. Liu, D. Khim and Y.-Y. Noh, *Phys. Chem. Chem. Phys.*, 2015, **17**, 26553–26574.
9 S. Holliday, J. E. Donaghey and I. McCulloch, *Chem. Mater.*, 2014, **26**, 647–663.
10 S.-H. Liao, H.-J. Jhuo, P.-N. Yeh, Y.-S. Cheng, Y.-L. Li, Y.-H. Lee, S. Sharma and S.-A. Chen, *Sci. Rep.*, 2014, **4**, 6813.
11 Y. Liu, J. Zhao, Z. Li, C. Mu, W. Ma, H. Hu, K. Jiang, H. Lin, H. Ade and H. Yan, *Nat. Commun.*, 2014, **5**, 5293.
12 M. A. Green, K. Emery, Y. Hishikawa, W. Warta and E. D. Dunlop, *Prog. Photovoltaics*, 2016, **24**, 3–11.
13 C.-H. Peters, I. T. Sachs-Quitana, J. P. Kastrop, S. Beaupré, M. Leclerc and M. D. McGehee, *Adv. Energy Mater.*, 2011, **1**, 491–494.
14 W. R. Mateker, I. T. Sachs-Quintana, G. F. Burkhard, R. Cheacharoen and M. D. McGehee, *Chem. Mater.*, 2015, **27**, 404–407.
15 C. Luo, A. K. K. Kyaw, L. A. Perez, S. Patel, M. Wang, B. Grimm, G. C. Bazan, E. J. Kramer and A. J. Heeger, *Nano Lett.*, 2014, **14**, 2764–2771.
16 Y. Zhang, E. Bovill, J. Kingsley, A. R. Buckley, H. Yi, A. Iraqi, T. Wang and D. G. Lidzey, *Sci. Rep.*, 2016, **6**, 21632.
17 S. Beaupré and M. Leclerc, *J. Mater. Chem. A*, 2013, **1**, 11097–11105.
18 K. Ziegler, E. Holzkamp, H. Breil and H. Martin, *Angew. Chem.*, 1995, **67**, 541–547.
19 G. Natta, P. Pino, P. Corradini, F. Danusso, E. Mantica, G. Mazzanti and G. Moraglio, *J. Am. Chem. Soc.*, 1955, **77**, 1708–1710.
20 D. Milstein and J. K. Stille, *J. Am. Chem. Soc.*, 1978, **100**, 3636–3638.
21 K. Tamao, K. Sumitami and M. Kumada, *J. Am. Chem. Soc.*, 1972, **94**, 4374–4376.

22 R. F. Heck and J. P. Nolley, *J. Org. Chem.*, 1972, **37**, 2320–2322.

23 A. Suzuki, *Angew. Chem., Int. Ed.*, 2011, **50**, 6723–6737.

24 E. Negishi, *Angew. Chem., Int. Ed.*, 2011, **50**, 6738–6764.

25 Y. Chauvin, *Angew. Chem., Int. Ed.*, 2006, **45**, 3741–3747.

26 R. R. Schrock, *Angew. Chem., Int. Ed.*, 2006, **45**, 3748–3759.

27 R. H. Grubbs, *Angew. Chem., Int. Ed.*, 2006, **45**, 3760–3765.

28 A. Facchetti, L. Vaccaro and M. Assunta, *Angew. Chem., Int. Ed.*, 2012, **51**, 3520–3523.

29 S. Kowalski, S. Allard, K. Zilberberg, T. Riedl and U. Scherf, *Prog. Polym. Sci.*, 2013, **38**, 1805–1814.

30 J.-R. Pouliot, F. Grenier, J. T. Blaskovits, S. Beaupré and M. Leclerc, *Chem. Rev.*, 2016, **116**, 14225–14274.

31 A. E. Rudenko and B. C. Thompson, *J. Polym. Sci., Part A: Polym. Chem.*, 2015, **53**, 135–147.

32 T. Bura, P.-O. Morin and M. Leclerc, *Macromolecules*, 2015, **48**, 5614–5620.

33 P.-O. Morin, T. Bura and M. Leclerc, *Mater. Horiz.*, 2016, **3**, 11–20.

34 T. Bura, J. T. Blaskovits and M. Leclerc, *J. Am. Chem. Soc.*, 2016, **138**, 10056–10071.

35 M. Sévignon, J. Papillon, E. Schulz and M. Lemaire, *Tetrahedron Lett.*, 1999, **40**, 5873–5876.

36 Q. Wang, R. Takita, Y. Kikuzaki and F. Ozawa, *J. Am. Chem. Soc.*, 2010, **132**, 11420–11421.

37 S. Hayashi, Y. Kojima and T. Koizumi, *Polym. Chem.*, 2015, **6**, 881–885.

38 A. E. Rudenko, A. A. Latif and B. C. Thompson, *Nanotechnology*, 2014, **25**, 014005.

39 J.-R. Pouliot, M. Wakioka, F. Ozawa, Y. Li and M. Leclerc, *Macromol. Chem. Phys.*, 2016, **217**, 1493–1500.

40 S. Beaupré, A. Pron, S. H. Drouin, A. Najari, L. Mercier, A. Robitaille and M. Leclerc, *Macromolecules*, 2012, **45**, 6906–6914.

41 X. Wang and M. Wang, *Polym. Chem.*, 2014, **5**, 5784–5792.

42 G. Marzano, D. Kotowski, F. Badudri, R. Musio, A. Pellegrino, S. Luzzati, R. Po and G. M. Farinola, *Macromolecules*, 2015, **48**, 7039–7048.

43 P. Berrouard, A. Najari, A. Pron, D. Gendron, P.-O. Morin, J.-R. Pouliot, J. Veilleux and M. Leclerc, *Angew. Chem., Int. Ed.*, 2012, **51**, 2068–2071.

44 J. Jo, A. Pron, P. Berrouard, W. L. Leong, J. D. Yuen, J. S. Moon and M. Leclerc, *Adv. Energy Mater.*, 2012, **2**, 1397–1403.

45 A. Pron, P. Berrouard and M. Leclerc, *Macromol. Chem. Phys.*, 2013, **214**, 7–16.

46 L. G. Mercier, B. R. Aïch, A. Najari, S. Beaupré, P. Berrouard, A. Pron, A. Robitaille, Y. Tao and M. Leclerc, *Polym. Chem.*, 2013, **4**, 5252–5260.

47 J.-R. Pouliot, L. G. Mercier, S. Caron and M. Leclerc, *Macromol. Chem. Phys.*, 2013, **214**, 453–457.

48 Q. Guo, J. Dong, D. Wan, D. Wu and J. You, *Macromol. Rapid Commun.*, 2013, **34**, 522–527.

49 P. Sonar, T. R. B. Foong and A. Dodabalapur, *Phys. Chem. Chem. Phys.*, 2014, **16**, 4275–4283.

50 J.-R. Pouliot, B. Sun, M. Leduc, A. Najari, Y. Li and M. Leclerc, *Polym. Chem.*, 2015, **6**, 278–282.

51 S. Broll, F. Nübling, A. Luzio, D. Lentzas, H. Komber, M. Caironi and M. Sommer, *Macromolecules*, 2015, **48**, 7481–7488.

52 M. Gruber, S.-H. Jung, S. Schott, D. Venkateshvaran, A. J. Kronemeijer, J. W. Andreasen, C. R. McNeill, W. W. H. Wong, M. Shahid, M. Heeney, J.-K. Lee and H. Sirringhaus, *Chem. Sci.*, 2015, **6**, 6949–6960.

53 Y. Gao, X. Zhang, H. Tian, J. Zhang, D. Yan, Y. Geng and F. Wang, *Adv. Mater.*, 2015, **27**, 6753–6759.

54 P. Homyak, Y. Liu, F. Liu, T. P. Russel and E. B. Coughlin, *Macromolecules*, 2015, **48**, 6978–6986.

55 E. Iizuka, M. Wakioka and F. Ozawa, *Macromolecules*, 2015, **48**, 2989–2993.

56 N. C. Bruno, M. T. Tudge and S. L. Buchwald, *Chem. Sci.*, 2013, **4**, 916–920.

57 A. E. Rudenko and B. C. Thompson, *Macromolecules*, 2015, **48**, 569–575.

58 A. S. Dubnik, T. J. Aldrich, N. D. Eastham, R. P. H. Chang, A. Facchetti and T. J. Marks, *J. Am. Chem. Soc.*, 2016, **138**, 15699–15709.

59 Z. Bao, W. K. Chan and L. Yu, *J. Am. Chem. Soc.*, 1995, **117**, 12426–12435.

60 N. Takeda, T. Tagawa and M. Unno, *Heterocycl. Chem.*, 2014, **25**, 628–635.

61 Q. Guo, J. Dong, D. Wan, D. Wu and J. You, *Macromol. Rapid Commun.*, 2013, **34**, 522–527.

62 P.-O. Morin, T. Bura, B. Sun, S. I. Gorelsky, Y. Li and M. Leclerc, *ACS Macro Lett.*, 2015, **4**, 21–24.

63 K. H. Hendriks, W. Li, G. H. L. Heintges, G. W. P. van Pruissen, M. M. Wienk and R. A. J. Janssen, *J. Am. Chem. Soc.*, 2014, **136**, 11128–11133.

64 M. Wakioka, S. Ishiki and F. Ozawa, *Macromolecules*, 2015, **48**, 8382–8388.

65 G. E. Morse, A. Tournebize, A. Rivaton, T. Chassé, C. Taviot-Gueho, N. Blouin, O. R. Lozman and S. Tierney, *Phys. Chem. Chem. Phys.*, 2015, **17**, 11884–11897.

66 H. Li, S. Sun, S. Mhaisalkar, M. T. Zin, U. M. L. Lam and A. C. Grimsdale, *J. Mater. Chem. A*, 2014, **2**, 17925–17933.

67 C. B. Nielsen, R. S. Ashraf, N. D. Treat, B. C. Schroeder, J. E. Donaghey, A. J. P. White, N. Stingelin and I. McCulloch, *Adv. Mater.*, 2015, **27**, 948–953.

68 N. Blouin, A. Pron, G. Morse, L. Nanson, M. Krompiec and S. Berny, WO2014/2020184 A1, 2014.

69 S. I. Gorelsky, D. Lapointe and K. Fagnou, *J. Org. Chem.*, 2012, **77**, 658–668.

70 C. Guo, J. Quinn, B. Sun and Y. Li, *Polym. Chem.*, 2016, **7**, 4515–4524.

71 K. Wang, G. Wang and M. Wang, *Macromol. Rapid Commun.*, 2015, **36**, 2162–2170.

72 Y. Gao, X. Zhang, H. Tian, J. Zhang, D. Yan, Y. Geng and F. Wang, *Adv. Mater.*, 2015, **27**, 6753–6759.

73 G. Marzano, F. Carulli, F. Babudri, A. Pellegrino, R. Po, S. Luzzati and G. M. Farinola, *J. Mater. Chem. A*, 2016, **4**, 17163–17170.